Ab initio LSDA and LSDA + *U* study of pure and Cd-doped cubic lanthanide sesquioxides

D. Richard,* E. L. Muñoz, and M. Rentería
Departamento de Física and Instituto de Física La Plata (IFLP, CONICET La Plata), Facultad de Ciencias Exactas, Universidad Nacional de La Plata, CC 67, 1900 La Plata, Argentina

L. A. Errico
Departamento de Física and Instituto de Física La Plata (IFLP, CONICET La Plata), Facultad de Ciencias Exactas, Universidad Nacional de La Plata, CC 67, 1900 La Plata, Argentina and Universidad Nacional del Noroeste de la Pcia. de Buenos Aires (UNNOBA), Monteagudo 2772, 2700 Pergamino, Argentina

A. Svane and N. E. Christensen
Department of Physics and Astronomy, University of Aarhus, DK-8000 Aarhus C, Denmark
(Received 4 July 2013; published 31 October 2013)

The electronic, structural, and hyperfine properties of pure and Cd-doped lanthanide (Ln) sesquioxides with the cubic bixbyite structure (Ln_2O_3, Ln ranging from La to Lu) have been studied using the full-potential augmented plane wave plus local orbital (APW + lo) method within the local spin density approximation (LSDA) and the Coulomb-corrected LSDA + U. In the case of the pure systems, our calculations show that LSDA + U gives a better representation of the band structure compared to LSDA. The predicted equilibrium structures and the electric field gradient (EFG) tensor at Ln sites were calculated and compared with those obtained by means of hyperfine techniques and with theoretical results obtained in In_2O_3, Sc_2O_3, and Lu_2O_3 reported in the literature. The origin of the EFG at Ln sites and the role played by the 4f electrons on this quantity are discussed. In the case of the Cd-doped systems, the APW + lo method (also within LSDA and LSDA + U) was applied to treat the electronic structure of the doped system. The role of the Ln 4f electrons on the EFG at Cd impurity sites, and other variables like structural distortions induced by the Cd impurity, were investigated in detail and are discussed and compared with available experimental results. An excellent agreement between the experimental and calculated EFGs was found for all Cd-doped systems.

DOI: 10.1103/PhysRevB.88.165206 PACS number(s): 61.72.S−, 71.15.Mb, 71.20.Ps, 76.80.+y

I. INTRODUCTION

The lanthanide (Ln) oxides occur naturally as sesquioxides (Ln_2O_3) with the exceptions of Tb (Tb oxide occurs naturally as Tb_4O_7 and transforms into TbO_2 under applied oxygen pressure) and Pr and Ce, which oxidize to PrO_2 and CeO_2 in the presence of air, respectively. These oxides are wide-gap materials and transparent in the visible region.[1] Depending on the radius of the cation, there are three polymorphs for Ln sesquioxides at low temperatures: the hexagonal phase (A type, space group P-3m1), the monoclinic phase (B type, $C/2m$), and the cubic phase (C type, Ia-3, bixbyite structure).

Sesquioxides with the bixbyite structure have broad technological significance, with applications ranging from radiation containment matrix[2] to diluted magnetic semiconductors.[3] They play a fundamental role in the processing of ceramics as additives for low-temperature sintering, as phase stabilizers,[4] and as catalysts for the synthesis of many other 4f materials.[5] Because of the photoluminescence properties of Ln elements, they are also important optical materials.[6] In addition, they have potential use as new gate insulators in metal-oxide-semiconductor structures.[7]

Due to their many technological applications (and for basic reasons), sesquioxides with the bixbyite structure have been intensively studied for more than 60 years. From the experimental point of view, hyperfine interaction techniques such as Mössbauer spectroscopy (MS), perturbed angular correlations (PAC), nuclear magnetic resonance (NMR), and nuclear quadrupole resonance (NQR) have been largely applied to the study of pure Ln sesquioxides, because different Ln isotopes can be used as probes in these kinds of experiments.[8–10] These hyperfine techniques enable the determination of the electric field gradient (EFG) tensor, a quantity that is extremely sensitive to small changes in the symmetry of the electronic charge density close to the probe nucleus (due to its r^{-3} dependence from the charge sources), which in turn reflects the probe chemistry with its neighborhood. In consequence, hyperfine techniques are among the most straightforward ways to probe the nature of Ln sites and obtain information about electronic and structural Ln environments at the subnanoscopic scale.

In addition to the hyperfine experiments performed with Ln isotopes as probes, the bixbyite group was largely characterized by means of PAC using the probe (^{111}In→)^{111}Cd.[11–19] In these experiments, the EFG is measured at an impurity site (^{111}Cd). Therefore, a realistic model that describes the EFG (a model that not only reproduces the experimental value but also provides information about its origin) should accurately determine the electronic configuration of the host perturbed by the presence of the impurity, taking properly into account the electronic and structural effects introduced by the impurity probe atoms.

On the theoretical side, Ln_2O_3 are challenging systems for the different methods of calculation. Electronic structure calculations based on density functional theory (DFT) have been successful in describing structural, electronic, and magnetic properties of solids with itinerant valence electrons. However,

the exchange and correlation effects included in the local spin density approximation (LSDA)[20] are insufficient to account for the strong correlation experienced by the localized $4f$ electrons of the Ln compounds. As a result, the strongly correlated and mainly localized $4f$ states in lanthanides are rendered itinerant by LSDA. A realistic theoretical description of Ln_2O_3 needs to take into account the strong on-site f-f interactions that push the $4f$ electrons toward localization. A popular, efficient, simple, and computationally inexpensive improvement of LSDA is the LSDA + U method.[21] In this approximation, the correlation absent in LSDA is reintroduced by an on-site Coulomb repulsion parameter U, to which an *a priori* value has to be assigned. Another approach to examine these systems is to apply the self-interaction-corrected (SIC) LSDA.[22] In this method, a separation of the f-electron manifold into localized and delocalized subsets can be done. The decision of whether an f electron is treated as localized or delocalized, i.e., participating in the bonding, is made on the ground of energetics.

The theoretical investigations on lanthanide oxides in general (and on the bixbyite group in particular) were confined to structural optimizations, optical and fundamental properties such as density of states (DOS), and band structures.[23] As far as we know, there are no calculations of hyperfine properties at Ln sites in Ln_2O_3 reported in the literature (magnetic hyperfine fields and EFGs at isolated Ln impurities in an Fe host lattice were reported by Torumba *et al.*[24]) Since experimental data for the EFG at Ln sites in Ln_2O_3 exists, it is interesting to perform such calculations. In this paper, we present full-potential augmented plane wave plus local orbital (APW + lo) calculations of electronic and structural properties and the EFGs at Ln sites of Ln_2O_3 in order to evaluate the applicability of LSDA and LSDA + U to the calculation of a sensitive quantity such as the EFG, and to answer the question as to which extent the occupancy of the Ln-$4f$ states affects the EFG. With this purpose, our results are compared with experimental results for the EFG reported in the literature and with our previous theoretical results obtained in the bixbyites In_2O_3, Sc_2O_3, and Lu_2O_3. In view of the results obtained in the Ln_2O_3 pure systems, we have extended our study to the case of the EFG at Cd impurities substitutionally located at the cation sites of the Ln_2O_3 series.

This paper is organized as follows. In Sec. II, we describe the crystal bixbyite structure shared by all lanthanides that will be studied from first principles. In Sec. III, we present the hyperfine parameters that are measured in the experiments analyzed here and used for comparison with our calculations. In Sec. IV, we describe the method of calculation and the different approximations used in this paper. Our results are presented in Sec. V, discussing first the structural, electronic, and hyperfine properties found in the pure systems (Sec. V A) and focusing subsequently on the results obtained in the Cd-doped sesquioxides (Sec. V B). Finally, summary and conclusions are given in Sec. VI.

II. THE BIXBYITE STRUCTURE

Under suitable conditions, Fe, Mn, Sc, In, Tl, Y, and all Ln elements form a sesquioxide. Below 2300 K, the Ln sesquioxides adopt three structure types.[25,26] For the light lanthanide elements, the hexagonal sesquioxide phase (A type) is adopted. For the heavier Ln elements, the cubic Mn_2O_3 phase (C type), also known as the bixbyite structure, is adopted. Sm_2O_3, Eu_2O_3, and Gd_2O_3 can be found in either the C-type or the B-type structure, which is a monoclinic distortion of the C-type structure. The phase stability and phase transitions with temperature or pressure for all Ln sesquioxides were summarized in Refs. 25, 27, and 28.

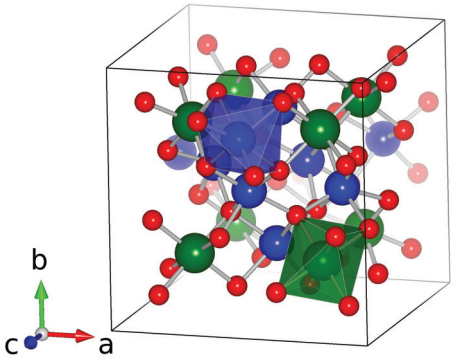

FIG. 1. (Color online) Bixbyite crystal structure. Small red spheres represent O anions, and large blue and green spheres represent Ln cations at sites C and D, respectively. The upper and lower polyhedra show the Ln coordination at sites C and D, respectively, with O_{NN}s.

The cubic bixbyite structure (Fig. 1) presents two inequivalent cationic sites, both O_6 coordinated. A quarter of these octahedral sites are centrosymmetric (C_{3i} point symmetry, site D), while the rest have a twofold symmetry (C_2 point symmetry, site C), giving a relative abundance $f_C/f_D = 3$. Site D can be viewed as a cation surrounded by six oxygen ions at the corners of a distorted cube, with two corners on the same diagonal vacant. All of these oxygen ions are at the same distance to the Ln cation (d_{NN}). In the case of site C, the cube is more distorted, the oxygen ions are missing across a face diagonal, and there are three pairs of d_{NN} values. The positions of all atoms in the unit cell can be defined by the four internal parameters u, x, y, and z, where u determines the positions of the cations at site C and x, y, and z determine those of the oxygen atoms.[29]

III. HYPERFINE PARAMETERS

Nuclear techniques, such as PAC, MS, and NQR, have been extensively applied to the study of materials. What is most rewarding about these methods is their "ability" to measure charge symmetry-related properties, such as the EFG, making it possible to obtain a fingerprint of the electronic configuration near and at the probe nucleus.[9]

The information provided by these techniques is given as a product of a nuclear and an external quantity. In the case of pure electric quadrupole interactions, the nuclear quantity is the nuclear quadrupole moment Q, characteristic of a given nuclear state of spin I, which interacts with the EFG present at the nuclear position. The EFG tensor is a rank two traceless symmetric tensor whose components, denoted by V_{ij}, are defined by the second derivative (with respect to the spatial coordinates) of the Coulomb potential $V(\boldsymbol{r})$ created by the charge density surrounding a given nucleus.[9] In the

principal axis system, the three diagonal components of the EFG tensor are labeled according to the conventional choice $|V_{xx}| \leqslant |V_{yy}| \leqslant |V_{zz}|$. Hence, V_{zz} is the component of the EFG tensor with the largest numerical value.

In the present paper, we will discuss experimental results obtained by means of different hyperfine techniques and using different probe nuclei. In the cases of the probes ^{44}Sc and ^{45}Sc (probes in PAC and NMR, respectively), ^{115}In and ^{175}Lu (probes in NQR experiments), and ^{111}Cd and ^{172}Yb (PAC probes), the measured quantity is the nuclear coupling constant ν_Q, related to V_{zz} by

$$\nu_Q = \frac{eQ\,V_{zz}}{h}. \tag{1}$$

Since the diagonal EFG tensor is traceless, it is completely determined by V_{zz} and the asymmetry parameter η:

$$\eta = \frac{V_{xx} - V_{yy}}{V_{zz}}. \tag{2}$$

According to the previously mentioned convention, $0 \leqslant \eta \leqslant 1$.

In the cases of the MS probes ^{155}Gd, ^{161}Dy, ^{169}Tm, ^{170}Yb, ^{171}Yb, ^{172}Yb, and ^{174}Yb, the measured quantity is the quadrupole splitting (ΔE_Q). In general, due to the nuclear spin (I) of the sensitive state of each MS probe, a separate experimental determination of V_{zz} and η is not possible. For example, for the $I = 3/2$ state in ^{155}Gd and ^{169}Tm, ΔE_Q is related to V_{zz} and η by

$$\Delta E_Q = \frac{eQ}{2} V_{zz} \left(1 + \frac{\eta^2}{3}\right)^{1/2}. \tag{3}$$

IV. METHOD OF CALCULATION

We performed spin-polarized *ab initio* electronic structure calculations to determine the self-consistent potential and the charge density inside the Ln_2O_3 and Cd-doped Ln_2O_3 cells. From these first-principles calculations, the hyperfine parameters at an indigenous Ln atom and at a Cd impurity replacing Ln cations were obtained, in the latter case taking properly into account the structural and electronic effects introduced by the impurity in the host lattice.

In the case of the pure Ln_2O_3 compounds, DFT-based[30] calculations have been performed with the APW + lo method,[31] as embodied in the WIEN2k code,[32] using the 40-atom Ln_2O_3 primitive cell. Exchange and correlation effects were treated using LSDA.[20] For some selected cases, the generalized gradient approximation (GGA) was applied using the Wu and Cohen[33] and the Perdew-Burke-Ernzerhof[34] parameterization of GGA. In order to take into account the strong on-site f-f correlation, LSDA plus the Hubbard U term (LSDA + U), in the SIC scheme[21] was employed. LSDA + U is not a fully *ab initio* method, because we have to select *a priori* the on-site Coulomb energy U.[35] In this paper, we took $U = 10.9$ eV (0.8 Ry) for the Ln-4f orbitals,[24,36] after having checked that the results do not depend significantly on its variation between 0.4 and 0.9 Ry. We also considered the spin-orbit coupling (SOC) for Ln atoms, using the scalar relativistic wave functions as its basis.[32] We did not add relativistic $5p(1/2)$ local orbitals to the scalar-relativistic APW + lo basis, as this can perturb the EFG values.

The parameter $R_{\rm mt}K_{\rm max}$, which controls the size of the basis set, was fixed to 7. $R_{\rm mt}$ is the smallest muffin-tin radius, and $K_{\rm max}$ is the largest wavenumber of the basis set. Integration in the reciprocal space was performed using the tetrahedron method, taking up to 100 k points in the first Brillouin zone. In all cases, we fixed the lattice parameters to the experimental values and determined the equilibrium internal atomic positions. To obtain the relaxed structures, once self-consistency of the potential was achieved, the forces on the atoms were obtained and the ions were displaced until the forces were below a tolerance value of 0.05 eV/Å. We use this tolerance criterion because a displacement induced by forces smaller than this limit produces changes in the internal coordinates that are below the convergence error. The diagonal elements of the EFG tensor were obtained directly from the V_{2M} components of the lattice harmonic expansion of the self-consistent potential.[37]

To check the precision of the present results, we performed several additional calculations. For selected systems, we increased the basis set (number of plane waves) and the number of k points, and we studied the effect of the muffin-tin radii on the relevant electronic and structural properties of the systems under study. With these studies, we have checked that EFGs and interatomic distances can be obtained with adequate precision when using the parameters detailed in the preceding paragraph.

This procedure was also used to study the Cd-doped cases, using the same basis set and k-point sampling. In order to calculate from first principles the electronic structure of Cd-doped Ln_2O_3 and the hyperfine parameters at the Cd sites, taking into account the structural and electronic effects introduced by the impurity in the host lattice, we considered the primitive cells of the Ln_2O_3 compounds periodically repeated containing a single Cd impurity located at cationic sites D or C. The replacement of a Ln atom in the cell by a Cd atom leads to an ordered compound, $Ln_{1.875}Cd_{0.125}O_3$, representing ~6 at.% doping. Additional calculations were performed using a larger impurity dilution. These additional calculations show that although 6 at.% doping is large compared to the parts per million dilutions used in the PAC experiments, the choice of the 40-atom unit cells keeps the Cd atoms sufficiently far from each other (on the order of 10 Å) to avoid significant Cd-Cd interaction. Thus, this is an excellent compromise between computational efforts and accuracy of the calculations.

The substitution of Ln atoms by Cd produces nonnegligible forces on its nearest neighbors. Since even small changes in the atomic positions can induce large effects on the EFG principal components, full relaxation of all atomic positions was also carried out in these doped cases until forces on the atoms were below 0.05 eV/Å.

Finally, and in order to study how the hyperfine parameters depend on small variations of the lattice structure, for some selected doped systems we obtained (by energy minimization) the equilibrium lattice parameters. In all cases, our calculations predict lattice parameters 2%–3% smaller than the experimental ones, in agreement with other theoretical results.[23] We found that the changes in V_{zz} components are smaller than 10% when going from the experimental to the equilibrium structures predicted by APW + lo. This difference is within the precision limit of the calculation. Therefore, we

decided to keep the lattice parameters fixed at the experimental values.

V. RESULTS AND DISCUSSION

A. Pure Ln_2O_3

In the following, we will separate the systems under study in three groups: (1) In_2O_3 and Sc_2O_3 (cations that do not have f shells), (2) Lu_2O_3 and La_2O_3 (closed f shell in the Lu^{+3} configuration and empty f shell in the La^{+3} configuration), and (3) Ce_2O_3, Pr_2O_3, Nd_2O_3, Pm_2O_3, Sm_2O_3, Eu_2O_3, Gd_2O_3, Tb_2O_3, Dy_2O_3, Ho_2O_3, Er_2O_3, Tm_2O_3, and Yb_2O_3 (partially filled f shell in the Ln^{+3} configuration). *Ab initio* predictions for the EFG at In and Sc sites in both oxides were reported in Refs. 38 and 39, so we simply summarize their main results here. Ce_2O_3, Pr_2O_3, and Tb_2O_3 do not occur naturally (as we said before, Ce, Pr, and Tb oxidize only to CeO_2, PrO_2, and TbO_2), and the C form of La_2O_3, Nd_2O_3, and Pm_2O_3 is probably metastable or stabilized by certain impurities.[25] In these cases, and in order to complete the EFG systematics, we obtained the APW + lo equilibrium bixbyite structures predicted for these oxides.

The calculated DOSs of Sc_2O_3 and In_2O_3 are shown in Fig. 2. The overall band structures obtained here are consistent with previous theoretical results obtained in other isomorphous Ln sesquioxides.[23,40] The different approximations used for the exchange and correlation energy predict a similar direct (minimum) band gap at the Γ point for each system, which is ∼4.0 eV for Sc_2O_3 and 1.2 eV for In_2O_3 (Fig. 3). These predicted band gaps are smaller than the experimental ones (6 and 3 eV for Sc_2O_3 and In_2O_3, respectively). This

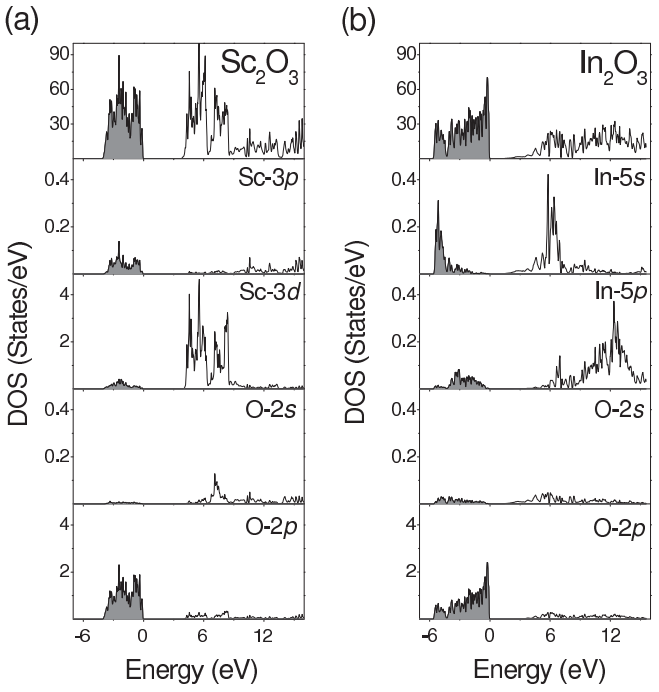

FIG. 2. Calculated total and atom-projected DOSs predicted by LSDA for (a) Sc_2O_3 and (b) In_2O_3. Shaded areas indicate occupied energy states. Different scales were used on the y axes to optimize visibility in all graphs.

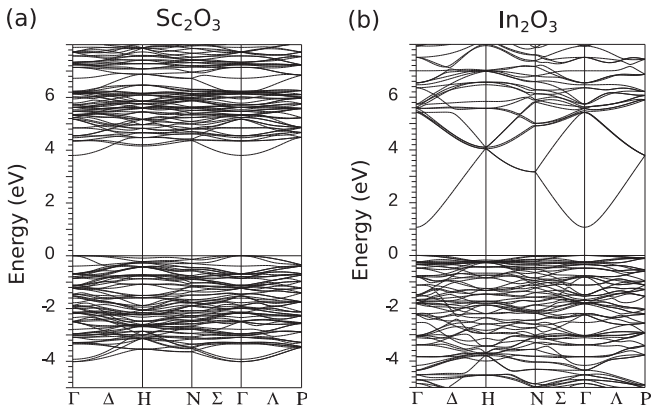

FIG. 3. Calculated band structure for (a) Sc_2O_3 and (b) In_2O_3. Zero energy is at the top of the valence band, denoted by a solid horizontal line.

underestimation reflects the well-known deficiency of LSDA and GGA to predict experimental band gaps,[41] but this does not invalidate the fine structure of the DOS and the calculation of observables, which depend only on the ground state as, for example, the EFG and the equilibrium structures.

As can be seen in Fig. 2, the valence bands of Sc_2O_3 and In_2O_3 are dominated by O-2p states, with a smaller contribution of cation orbitals, in agreement with the predominantly ionic nature of these sesquioxides.[42] The conduction band of Sc_2O_3 has a predominantly Sc-3d character with an admixture of O-2p states [Fig. 2(a)]. In the case of In_2O_3, this band is predominantly In-5s and In-5p with an admixture of O-2p states [Fig. 2(b)].

In the sesquioxides of group 2, the DOS predicted by LSDA for La_2O_3 consists of a valence band with a mainly O-2p character, while the La-4f states lie above the Fermi energy (E_F), forming the conduction band with La-5d states [Fig. 4(a)]. This result is in excellent agreement with those reported in Ref. 23. Our calculations predict an energy gap of 4.0 eV, which is 1.5 eV below the experimental value.[43] As expected, when the U correction is applied, the empty f band is shifted to higher energies [Fig. 4(b)]. In the case of Lu_2O_3, the DOS obtained using LSDA is shown in Fig. 4(c). The conduction band is composed of Lu-5d states. The valence band has an O-2p character, with the completely filled Lu-4f narrow band located at the top of this band. The DOS obtained using LSDA + U is presented in Fig. 4(d). As can be seen, the effect of U is to localize these f states 2 eV below the valence band, but the energy band gap is not changed. In this way, both LSDA and LSDA + U calculations predict a band gap of 3.4 eV, while the experimental value is 5.5 eV.[43] As a first conclusion, our calculations predict an insulating ground state for In_2O_3, Sc_2O_3, La_2O_3, and Lu_2O_3 that is in agreement with the experimental data.

In the case of the third group of sesquioxides (lanthanides with incomplete 4f shells in their +3 state), the DOSs for all sets of sesquioxides calculated with LSDA are quite similar. Representative examples are shown in Fig. 5(a). In all cases, the broad band below E_F originates from the O-2p states. LSDA also predict a partially filled Ln-4f peak located in the gap between the valence band and the Ln-5d states. This 4f

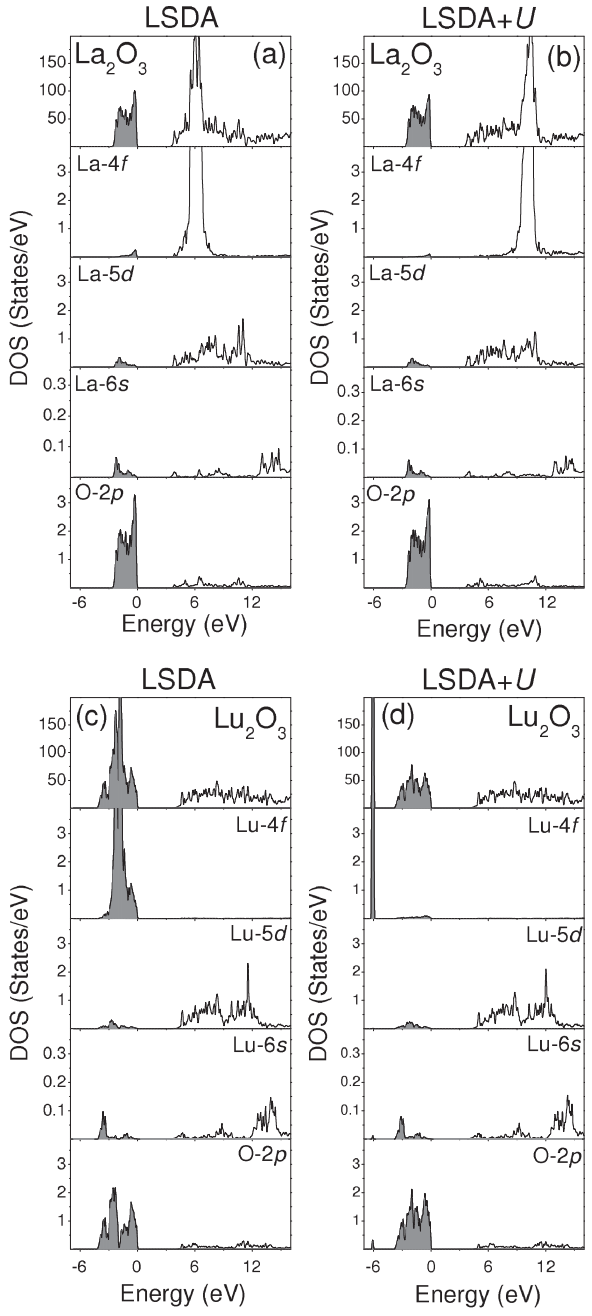

FIG. 4. Calculated total and atom-projected DOS using (a) LSDA and (b) LSDA + U for La_2O_3 and (c) LSDA and (d) LSDA + U for Lu_2O_3. Shaded areas indicate occupied energy states. Different scales were used on the y axes to optimize visibility in all graphs.

band is gradually filled as the number of f electrons of the Ln cation increases. For Gd_2O_3, where the cation is in the middle of the lanthanide series with the $4f^7$ configuration, the $4f$-up band is completely filled and the $4f$-down band is completely empty, in accordance with Hund's first rule.

The narrow f band at E_F leads to a metallic ground state in all cases (with the exception of Gd_2O_3). This result is in agreement with previous LSDA calculations[23] but disagrees with the experimental results. Thus, LSDA fails to predict the correct insulating ground state of the Ln sesquioxides with partially occupied $4f$ states in its +3 state.

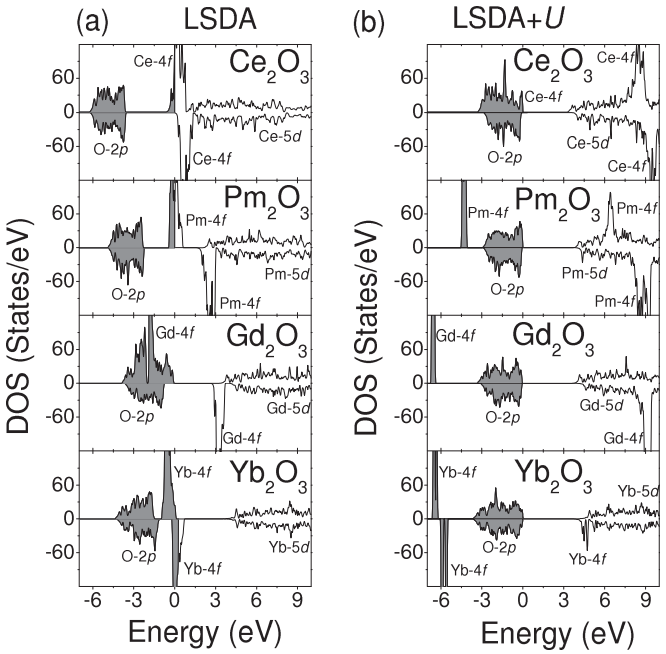

FIG. 5. Calculated total spin-resolved DOS by (a) LSDA and (b) LSDA + U in different lanthanide sesquioxides. Shaded areas indicate occupied energy states.

In order to improve the LSDA description of Ln_2O_3, LSDA + U calculations were performed. The Coulomb correction splits the $4f$ band into two subbands: the occupied $4f$ states are pushed well below E_F, and the unoccupied $4f$ states are shifted to higher energies so that these two subbands are separated by U, making sesquioxide insulators [Fig. 5(b)]. Now it is possible to distinguish a valence band with a predominantly O-$2p$ character and a conduction band with a Ln-$5d$ character separated by ∼4 eV.

In Table I, the theoretically predicted internal parameters u, x, y, and z are presented. Good agreement is seen when they are compared to the experimental results. In addition, it can be seen that the localization of the f electrons does not produce any significant difference in the internal parameters. The internal parameters were obtained with the lattice parameters fixed at the experimental ones.

Now we can focus on the hyperfine properties. In Table II and Fig. 6, we present the results for the EFG at both cationic sites of Sc_2O_3, In_2O_3, and Ln_2O_3 oxides. The results were obtained using the equilibrium structures predicted by LSDA and LSDA + U. We observe that LSDA predicts that the values of V_{zz} and η at each cationic site of the Ln_2O_3 series are almost independent of the cation considered (Fig. 6 and Table II). In the case of LSDA + U, the behavior of V_{zz} and η is more disperse. As a general conclusion, we can see that LSDA and LSDA + U predict similar hyperfine parameters (the largest differences between both approximations are found for both cationic sites of Ho_2O_3 and Dy_2O_3). In all cases, $|V_{zz}^D|/|V_{zz}^C| \approx 1.8$ [see solid lines in Fig. 6(c)], as could be expected from the geometry of the cationic sites[57] (V_{zz}^D and V_{zz}^C are the values of the EFG major component at sites D and C, respectively).

In order to understand the origin of the EFG tensor, we have to take into account that it is directly related to the anisotropy of the electronic density in the vicinity of the nucleus of

TABLE I. APW + lo structural internal parameters for *C*-type Ln_2O_3 calculated (for the lattice parameter *a* fixed to an experimental value) within LSDA and LSDA + *U*.[a]

		a (Å)	*u*	*x*	*y*	*z*
La_2O_3	Exp[29]	11.38				
	LSDA		−0.0294	0.3878	0.1470	0.3788
	LSDA + *U*		−0.0291	0.3882	0.1472	0.3790
Ce_2O_3	Exp[1]	11.16				
	LSDA		−0.0231	0.3838	0.1454	0.3801
	LSDA + *U*		−0.0282	0.3900	0.1478	0.3775
Pr_2O_3	Exp[44]	11.147(8)	−0.0290	0.385	0.155	0.382
	LSDA		−0.0282	0.3848	0.1468	0.3798
	LSDA + *U*		−0.0297	0.3884	0.1485	0.3784
Nd_2O_3	Exp[44]	11.074 (14)				
	LSDA		−0.0305	0.3853	0.1475	0.3804
	LSDA + *U*		−0.0310	0.3886	0.1491	0.3796
Pm_2O_3	Exp[44]	10.99(1)				
	LSDA		−0.0312	0.3852	0.1479	0.3812
	LSDA + *U*		−0.0310	0.3893	0.1488	0.3791
Sm_2O_3	Exp[45]	10.9085				
	LSDA		−0.0330	0.3859	0.1488	0.3812
	LSDA + *U*		−0.0311	0.3893	0.1492	0.3802
Eu_2O_3	Exp[45]	10.8245				
	LSDA		−0.0329	0.3860	0.1495	0.3814
	LSDA + *U*		−0.0318	0.3892	0.1499	0.3800
Gd_2O_3	Exp[45]	10.7970				
	LSDA		−0.0337	0.3862	0.1500	0.3815
	LSDA + *U*		−0.0320	0.3900	0.1500	0.3794
Tb_2O_3	Exp[1]	10.730(1)				
	LSDA		−0.0344	0.3863	0.1503	0.3819
	LSDA + *U*		−0.0320	0.3901	0.1500	0.3794
Dy_2O_3	Exp[46]	10.6706(7)	−0.03163(2)	0.3905(2)	0.1516(2)	0.3802(2)
	LSDA		−0.0336	0.3868	0.1499	0.3813
	LSDA + *U*		−0.0332	0.3899	0.1512	0.3803
Ho_2O_3	Exp[46]	10.606(2)	−0.03199(2)	0.3908(3)	0.1516(2)	0.3798(2)
	LSDA		−0.0347	0.3876	0.1519	0.3816
	LSDA + *U*		−0.0336	0.3896	0.1515	0.3803
Er_2O_3	Exp[47]	10.550	−0.03249	0.3910	0.1521	0.3786
	LSDA		−0.0353	0.3879	0.1525	0.3819
	LSDA + *U*		−0.0327	0.3899	0.1508	0.3799
Tm_2O_3	Exp[44]	10.485(5)	−0.033	0.392	0.153	0.377
	LSDA		−0.0346	0.3886	0.1530	0.3817
	LSDA + *U*		−0.0331	0.3907	0.1511	0.3800
Yb_2O_3	Exp[47]	10.432	−0.03253	0.3910	0.1523	0.3807
	LSDA		−0.0325	0.3892	0.1515	0.3810
	LSDA + *U*		−0.0332	0.3900	0.1515	0.3803
Lu_2O_3	Exp[45]	10.3847				
	LSDA		−0.0341	0.3906	0.1518	0.3804
	LSDA + *U*		−0.0336	0.3903	0.1520	0.3804

[a]Experimental structural data were extracted from the indicated references.

the probe atom where the EFG is measured or calculated. Within the theoretical approach, we will focus on the valence contribution to the EFG, i.e., the contribution originating from the nonspherically symmetric electron density of the valence and semicore electrons within the muffin-tin sphere of the probe atom. This contribution to the EFG dominates, while the lattice term (originating from more distant regions of the crystal) is almost negligible. This last contribution accounts for less than 5% of the total EFG. The dominant valence contribution can be further decomposed according to the different orbital symmetries.[37]

As expected, for La_2O_3 and Lu_2O_3, where the $4f$ shell is empty and completely filled, respectively, the $4f$ contribution to the EFG (V_{zz}^{ff}) is zero. We also found $V_{zz}^{ff} \approx 0$ in the case of Gd_2O_3, a result in agreement with the spherically symmetric half-filled $4f$ shell. In these sesquioxides, and in Sc_2O_3 and In_2O_3, the *p* contribution to the EFG (V_{zz}^{pp}) dominates over the *d* contribution, while the mixed *s*-*d*, *s*-*p*,

TABLE II. Theoretical and experimental values for the numerically largest principal component V_{zz} (in units of 10^{21} V/m^2) and the asymmetry parameter η of the EFG at both cationic sites of Sc_2O_3, In_2O_3, and the Ln_2O_3 oxides.[a]

		Theoretical results (this paper)				Experimental results			
		LSDA		LSDA + U					
		V_{zz}	η	V_{zz}	η	Method	T[b]	V_{zz}^{exp}[c]	η
Site C	Sc_2O_3	−3.0[39]	0.52[39]			PAC[39]	300	2.741(7)	0.630(3)
						NMR[48]		2.9(1)	0.63(1)
	In_2O_3	+5.5[19]	0.94[19]			NQR[49]	77	6.51	0.9246
	La_2O_3	−13.5	0.43	−13.4	0.47				
	Ce_2O_3	−13.1	0.73	−11.0	0.42				
	Pr_2O_3	−13.2	0.51	−11.3	0.55				
	Nd_2O_3	−13.7	0.44	−13.7	0.45				
	Pm_2O_3	−14.9	0.51	−12.8	0.38				
	Sm_2O_3	−14.3	0.45	−13.7	0.65				
	Eu_2O_3	−14.4	0.53	−14.0	0.40				
	Gd_2O_3	−14.4	0.52	−14.1	0.42	MS[50]	4.2	11.7(9)	
	Tb_2O_3	−14.9	0.51	−12.2	0.31				
	Dy_2O_3	−13.6	0.48	−10.2	0.85	MS[51]	7	18.4	
	Ho_2O_3	−13.7	0.59	−14.2	0.48				
	Er_2O_3	−13.5	0.65	−14.9	0.39				
	Tm_2O_3	−12.9	0.73	−13.7	0.70	MS[52]	1.8	29(2)	
	Yb_2O_3	−12.9	0.61	−15.1	0.55	MS[53]	20	−32.1(1.4)	0.11(3)
						MS[54]	4.2	33.5(1)	0.10(4)
						PAC[55]	78	33.0(5)	0.09(1)
	Lu_2O_3	−14.7	0.41	−14.7	0.41	NQR[49]	77	14.42	0.5861
Site D	Sc_2O_3	+4.8[39]	0.00[39]			PAC[39]	300	4.19(2)	0.00[d]
						NMR[48]		4.4(2)	0.00
	In_2O_3	+8.4[19]	0.00[19]			NQR[49]	77	9.35	0.0153
	La_2O_3	+27.0	0.00	+26.2	0.00				
	Ce_2O_3	+24.2	0.00	+26.4	0.00				
	Pr_2O_3	+25.3	0.00	+25.6	0.00				
	Nd_2O_3	+25.6	0.00	+26.6	0.00				
	Pm_2O_3	+26.0	0.00	+24.5	0.00				
	Sm_2O_3	+25.5	0.00	+23.8	0.00				
	Eu_2O_3	+25.1	0.00	+25.9	0.00				
	Gd_2O_3	+24.7	0.00	+26.6	0.00	MS[50]	4.2	22(2)	
	Tb_2O_3	+24.5	0.00	+24.8	0.00				
	Dy_2O_3	+24.7	0.00	+31.2	0.00	MS[51]	7	33.0	
	Ho_2O_3	+23.7	0.00	+29.7	0.00				
	Er_2O_3	+22.7	0.00	+23.8	0.00				
	Tm_2O_3	+22.0	0.00	+19.7	0.00	MS[52]	1.8	37(3)	
	Yb_2O_3	+23.9	0.00	+25.4	0.00	MS[53]	20	−12.8(1.1)	0.54(14)
						MS[54]	4.2	14.8(4)	0.00[d]
						PAC[55]	78	15.0(5)	0.00[d]
	Lu_2O_3	+26.3	0.00	+26.5	0.00	NQR[49]	77	25.96	0.0127

[a]In order to derive V_{zz} from the nuclear coupling constant ν_Q or the quadrupole splitting ΔE_Q, we used Eqs. (1) and (3), respectively, and the nuclear quadrupole moments Q reported in Ref. 56.

[b]T values are expressed in Kelvins.

[c]The signs of V_{zz}^{exp} are unknown except in the case of the MS experiments performed in Yb_2O_3 by Plingen *et al.* (Ref. 53). Due to the characteristics of the probes employed in the MS experiments, η cannot be determined (see text).

[d]The η parameter is fixed during the fitting procedure.

and p-f contributions are practically negligible. The EFG contribution originating from the p wave functions dominates over the d contribution, because the first node of the p wave function is at a distance from the cation nucleus that is much shorter than the first node of the d wave function. In addition, even a small p-charge anisotropy can produce a large V_{zz}^{pp} contribution to the EFG. The V_{zz}^{pp} originates mainly from the O p bands, where tails of O p states extend into the Ln atomic spheres and contribute to the Ln p character.

In the case of the Ln_2O_3 sesquioxides with incomplete $4f$ shells in their 3+ configuration, the V_{zz}^{pp} contribution to the EFG at the Ln sites also dominates over the d contribution, and the mixed terms are almost negligible. Concerning the f contribution to the EFG, LSDA predicts that V_{zz}^{pp} dominates

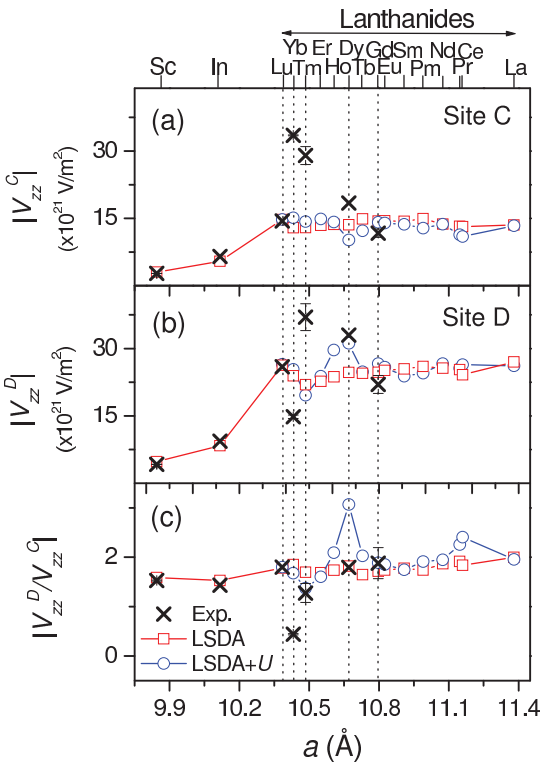

FIG. 6. (Color online) Theoretical and experimental (crosses) EFG results for pure Sc_2O_3, In_2O_3, and Ln_2O_3 oxides as a function of lattice parameter a (the respective Ln atom labels are indicated on the top): (a) $|V_{zz}^C|$, (b) $|V_{zz}^D|$, and (c) $|V_{zz}^D/V_{zz}^C|$. Open squares and circles correspond to LSDA and LSDA + U, respectively. *Ab initio* results for In_2O_3 and Sc_2O_3 are those reported in Refs. 19 and 39, respectively. Experimental results were extracted from Refs. 39 and 48–55.

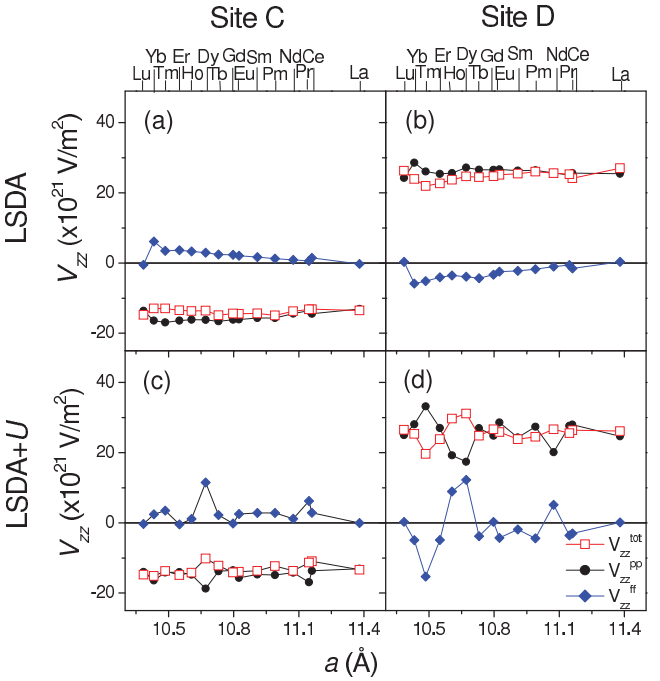

FIG. 7. (Color online) Main contributions to V_{zz} at both cationic sites for the Ln_2O_3 series, using LSDA at (a) site C and (b) site D and LSDA + U at (c) site C and (d) site D as a function of the lattice parameter a (Ln atoms are indicated on the top).

over V_{zz}^{ff} (Fig. 7). In addition, V_{zz}^{pp} and V_{zz}^{ff} have opposite signs and their magnitudes monotonously decrease at both crystallographic cation sites with increasing lattice parameter a, maintaining a nearly constant total V_{zz} through the lanthanide series [Fig. 7(a) and 7(b)]. In the case of LSDA + U, for some sesquioxides (Tm_2O_3 and Dy_2O_3), the magnitudes of V_{zz}^{pp} and V_{zz}^{ff} are comparable [Fig. 7(c) and 7(d)]. In these cases, the changes in V_{zz}^{ff} are "compensated" for by the changes of V_{zz}^{pp}. In consequence, the EFG systematics predicted by LSDA + U is qualitatively the same as those predicted by LSDA. This correlation between the two contributions to the EFG was first suggested by Torumba *et al.*[24] who studied hyperfine fields at Ln impurities in Fe. They also found a strong $5p$ contribution to the EFG and that in general V_{zz}^{ff} and V_{zz}^{pp} have opposite signs. When SOC is included in the LSDA and LSDA + U approaches, only insignificant changes in the EFG values are found (the differences in V_{zz} are below 10%).

Before comparing the present theory with available experimental results, we will discuss the experimental data set for the EFG. The PAC technique was applied to the study of the nuclear quadrupole interactions of the first excited $I = 1$ state of (^{44}Ti→)^{44}Sc in Sc_2O_3 at 300 K.[39] Two hyperfine interactions were found, one asymmetric and the other one (the less populated) axially symmetric, the frequency ν_Q of the axially symmetric interaction being twice as large as that of the asymmetric one. *Ab initio* calculations enabled the assignment of these interactions to ^{44}Sc probes located at sites C and the D of the Sc_2O_3 host, respectively, and gave an explanation for the preferential occupation of the asymmetric cationic site C of the structure by the ^{44}Ti(→^{44}Sc) doping impurities. The results for the hyperfine parameters that characterize both interactions are listed in Table II. Similar results for the EFG tensor were obtained by Alba *et al.*[48] using NMR with the indigenous ^{45}Sc as probe atom.

Lu_2O_3 and In_2O_3 were measured by means of NQR using ^{115}In and ^{175}Lu as probes.[49] Both experiments were performed at 77 K. Again, two hyperfine interactions were found, with similar characteristics in both oxides, one asymmetric (η on the order of 0.6 for Lu_2O_3 and 0.9 for In_2O_3) and one axially symmetric, with V_{zz} of the axially symmetric interactions being larger than V_{zz} of the asymmetric one (Table II).

Few experimental data for the EFG at Ln sites in Ln_2O_3 are available, and these come from experiments that were performed at different temperatures. Since it is known that for these probes the EFG has strong variation with temperature (T),[8,58,59] we will compare our APW + lo results with those coming from low T measurements.[49–55]

For Gd_2O_3, Dy_2O_3, and Tm_2O_3, Mössbauer measurements were carried out using ^{155}Gd, ^{161}Dy, and ^{169}Tm as probes. In the cases of Gd_2O_3 and Tm_2O_3, due to the nuclear spin of the sensitive states of ^{155}Gd and ^{169}Tm ($I = 3/2$), the result of the Mössbauer experiments for each interaction is the quadrupole splitting ΔE_Q.[50,52] The common procedure to obtain V_{zz} from ΔE_Q is to fix $\eta = 0$ (Refs. 51, 60, and 61). ΔE_Q changes 12% going from $\eta = 0$ to $\eta = 1$, so we then estimated V_{zz}^{exp} from ΔE_Q, leaving its variation with η as the error bar. In

both experiments (performed at 4.2 K in the case of Gd_2O_3 and 1.8 K in the case of Tm_2O_3), two interactions were found. These interactions are characterized by a V_{zz} ratio on the order of 1.3–1.8 (Table II) and were associated to sites D (those characterized by a larger V_{zz} value) and C of the structures. In the case of Dy_2O_3, the $I = 5/2$ of the sensitive state of ^{161}Dy enables (in principle) the separate determination of V_{zz} and η. The predominant features of the spectra (taken at 2.5 K) are associated with probes located at sites C. For this interaction, η should be different from zero, but within the accuracy of the experiment, the effect of η on the value of V_{zz} was negligible and in consequence was taken to be zero for the fitting procedure. A second, weaker interaction was observed, with a quadrupole splitting larger than those associated to the C site. This second interaction is axially symmetric and was associated to probes at site D of the structure.

Yb_2O_3 is the bixbyite most deeply studied experimentally. EFG measurements at its cationic sites, both by MS,[53,54] using ^{170}Yb, ^{171}Yb, ^{172}Yb, and ^{174}Yb as probes, and by PAC spectroscopy,[55] with ^{172}Yb as probe, yield similar results: one interaction characterized by $|V_{zz}|$ on the order of 32×10^{21} V/m^2 and an η value on the order of 0.1 and a second interaction characterized by $|V_{zz}| = 12-15 \times 10^{21}$ V/m^2 and $\eta = 0.45$–0.65 (Table II). In these MS experiments, it is possible to determine, in addition to the magnitude and symmetry of the EFG, the sign of V_{zz} (Ref. 62), which turns out to be negative for both sites[53] (Table II). These experimental results for Yb_2O_3 follow the trend observed in other bixbyites. However, contrary to all previous cases, the interaction characterized by the large V_{zz} (in absolute value) and $\eta = 0.1$ was associated to the asymmetric site, and the interaction characterized by low V_{zz} and η on the order of 0.5 was associated to the axially symmetric site. This site assignment was proposed based on the intensity of the hyperfine interactions (the more intense must correspond to site C, the most abundant in the structure), while neither the asymmetry parameters nor the frequency ratios were considered.

NMR and MS experiments on La_2O_3 (using ^{139}La and ^{137}La as probes) were also reported in the literature.[49,61,63] But in one case, the results correspond to the hexagonal *A* phase (the stable one for this sesquioxide),[49,63] and in the case of the MS experiments (performed at room temperature), the authors observed only one interaction that was tentatively associated to site C of *C*-La_2O_3.[61] Hence these results are not directly comparable to the present calculations.

If we compare our APW + lo predictions with the experimental results (Table II and Fig. 6), we can see excellent agreement for Sc_2O_3, In_2O_3, and Lu_2O_3 (cations with no f shells or the $4f$ shell completely filled). In sesquioxides with cations that present a partially filled $4f$ shell, good agreement is also observed in the case of Gd_2O_3. Considering the accuracy and limitations of the experiments, the agreement is also reasonable in the case of Dy_2O_3.

For Tm_2O_3 we can observe in Fig. 6 and Table II that V_{zz}^D and V_{zz}^C are underestimated nearly by the same factor. The discrepancy could be attributed to two alternative factors: (1) The nuclear quadrupole moment Q of the sensitive state of ^{169}Tm could be overestimated, or (2) LSDA and LSDA + U provide a poor description of the electronic structure of this system. Concerning factor 1, the ratio $|V_{zz}^D|/|V_{zz}^C|$ predicted by APW + lo, which does not depend on Q, is in good agreement with the experimental result. For many important probe nuclei, the Q values are not known or are known with limited accuracy, and their determination is still an open field of research. An improved determination of the Q value of the Mössbauer sensitive states of ^{169}Tm could be of great interest.

Finally, we discuss the EFG at the Yb sites in Yb_2O_3. If we take as valid the site assignment of the hyperfine interactions observed in the PAC and MS experiments, the theory fails in the prediction of the EFG at both cationic sites: $|V_{zz}^C|$ is underestimated by LSDA and LSDA + U, and $|V_{zz}^D|$ is overestimated (Fig. 6). This discrepancy cannot be associated to a problem in the Q values of the probes. If we leave the assignment performed in the literature (which is based on the site abundance and the intensity of the hyperfine interactions) and we perform the assignment based on the symmetry of the sites, and on the experimental and theoretical systematics for the bixbyites, V_{zz}^{exp} should be $-13_1 \times 10^{21}$ V/m^2 and $\eta^{exp} = 0.54_{14}$ for site C ($V_{zz}^{\mathrm{LSDA}} = -12.9 \times 10^{21}$ V/m^2, $\eta^{\mathrm{LSDA}} = 0.61$, and $V_{zz}^{\mathrm{LSDA}+U} = -15.1 \times 10^{21}$ V/m^2, $\eta^{\mathrm{LSDA}+U} = 0.55$). For site D, V_{zz}^{exp} should be $-32_1 \times 10^{21}$ V/m^2 and $\eta^{exp} = 0.11_3$ ($V_{zz}^{\mathrm{LSDA}} = +23.9 \times 10^{21}$ V/m^2, $\eta^{\mathrm{LSDA}} = 0.00$, and $V_{zz}^{\mathrm{LSDA}+U} = +25.4 \times 10^{21}$ V/m^2, $\eta^{\mathrm{LSDA}+U} = 0.00$). With this assignment, the theory and experiment agreement is better, but APW + lo still fails to predict the correct sign of the EFG at site D, and the experimental site population is not in agreement with the natural abundance of sites C and D in the structure. We have to conclude that, independent of the site assignment, LSDA and LSDA + U fail in the description of the EFG at both cationic sites of Yb_2O_3.

In order to understand this failure, let us return to the experiments. In addition to the PAC and MS experiments performed at low temperatures, the temperature dependence of the EFG at the two cationic sites of Yb_2O_3 was studied by Rams and Królas.[55] They found a strong dependence of V_{zz}^C and V_{zz}^D on temperature. In perfect agreement with the results at 20 and 4.2 K reported in Refs. 53 and 54, respectively, they found that at low temperatures, V_{zz}^C is larger than V_{zz}^D [$|V_{zz}^D|/|V_{zz}^C| \approx 0.4$; Fig. 6(c)]. But at $T > 750$ K, V_{zz}^D becomes larger than V_{zz}^C($|V_{zz}^D|/|V_{zz}^C| \approx 2.0$), in qualitative agreement with our APW + lo calculations. This temperature dependence of the EFG in Yb_2O_3 was attributed to the Yb-$4f$ contribution to the EFG. In this picture, the $4f$ contribution to the EFG is dominant at low temperatures. But with increasing temperatures, the $4f$ levels are progressively populated, and for $T > 1300$ K, all $4f$ states are equally occupied and the $4f$ contribution to the EFG vanishes. In consequence, the 0-K APW + lo calculations (which predict a minor $4f$ contribution to the EFG) are in agreement with the experimental result obtained at high temperatures and may fail to describe the $4f$ states population at low temperatures. Unfortunately, PAC cannot give information about the sign of the EFG. In our opinion, new experimental data (measurements of the magnitude, symmetry, and sign of V_{zz}^D and V_{zz}^C as a function of T) are crucial to unraveling the electronic structure of Yb_2O_3 and to evaluating the validity of the LSDA and LSDA + U models. Similar experiments must be done in the entire Ln sesquioxides series and in particular in Tm_2O_3.

B. Cd-doped Ln_2O_3

In the previous section, we discussed the EFG results at Ln sites of Ln_2O_3. Among these cases, the EFG is measured or calculated at the nuclear site of atoms that have incomplete $4f$ shells. Therefore, the contribution of the $4f$ electrons to the EFG could be important. In addition to the experimental results obtained in the pure samples, Ln_2O_3 oxides with the bixbyite structure were largely studied by means of PAC using $^{111}In \rightarrow {}^{111}Cd$ as the probe. In this case, the probe is an impurity in the system under study, and it has no $4f$ electrons. Here, we used the APW + lo method to calculate the EFG at the Cd site. Now the Ln atoms (in other words, the Ln-$4f$ electrons) are far from Cd (at least in its second coordination shell) and not in the muffin-tin sphere of the probe atom, as was the case in the pure systems. We will present here results for Cd in Gd_2O_3, Dy_2O_3, Tm_2O_3, and Yb_2O_3. We will also include in the discussion the APW + lo predictions for Cd-doped Sc_2O_3,[64] In_2O_3,[38] Y_2O_3,[19] and Lu_2O_3[40] in order to give an answer to the question about to which extent the Ln-$4f$ electrons affect the EFG at the Cd sites.

To study Cd-doped Ln_2O_3, we followed the procedure described in Sec. III and in Refs. 64–66, replacing a Ln atom of type C or type D with a Cd atom. The first point to take into account in this problem is the charge state of the impurity system.[38,40,64–67] Since the valence of Cd is 2+, when a Cd atom replaces a Ln^{+3} atom in the structure, there is one electron less to fill the O-$2p$ band. The presence of the Cd impurity induces the appearance of a Cd-d character acceptor level at E_F, and the resulting system is metallic, as can be seen in Fig. 8(c). These states are spatially located at Cd and at their oxygen nearest-neighbor (O_{NN}) atoms. The questions are whether the real system we want to describe provides the lacking electron necessary to fill the impurity level and whether this point is relevant for the calculation. Based on the previously obtained results for other bixbyites,[38,40,64]

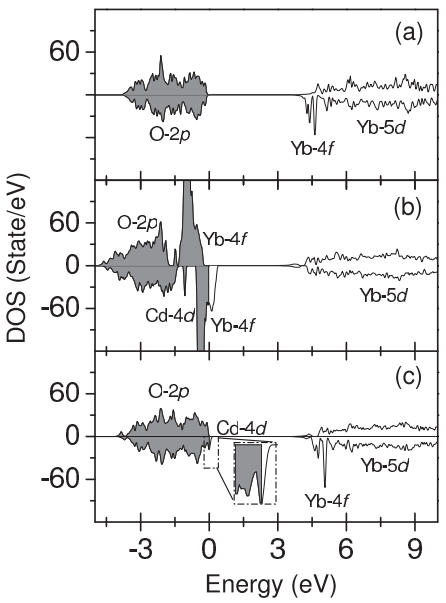

FIG. 8. Spin-resolved DOS for (a) pure Yb_2O_3 using LSDA + U and Cd-doped Yb_2O_3 using (b) LSDA and (c) LSDA + U. Shaded areas indicate occupied energy states. The magnified sector corresponds to the Cd acceptor level.

we will assume that the system provides the lacking electron [i.e., the impurity level at E_F is filled in Fig. 8(c)]. To describe this situation, we added one electron to the cell, and we compensated for the charge excess with a homogeneous positive background to obtain a neutral cell. A detailed study of the EFGs as a function of the charge state of the impurity will be presented in a forthcoming paper. In the cases of Gd_2O_3, Dy_2O_3, Tm_2O_3, and Yb_2O_3, the LSDA calculations present the problem of the delocalized $4f$ bands in the band gap previously discussed in pure Ln_2O_3 compounds [Fig. 8(b)], a problem that is corrected again using LSDA + U [Fig. 8(c)]. Here, the EFG is calculated at the Cd site, but the $4f$ band is spatially located at the Ln atoms, which are far from the point at which the EFG is calculated (or measured).

The substitution of a D-type Ln atom by a Cd impurity produces nonnegligible forces on the Cd-O_{NN}. As can be seen in Table III for the specific case of Cd in Yb_2O_3 (the other systems show the same behavior), the O_{NN}s relax outward along the Cd-O_{NN} directions, enlarging the Cd-O_{NN} bond lengths. The displacement of each of these O atoms is ∼0.1 Å in all cases (5% of the unrelaxed Cd-O_{NN} bond length). In the case of Cd replacing a C-type Ln, the magnitude of the structural relaxation is different for each of the three pairs of Cd-O_{NN} bond lengths but in average is similar to those produced at site D (5%). These enlargements of the bond lengths are in agreement with the picture that Cd tries to reconstruct the Cd-O_{NN} distances in its own oxide (Cd-O_{NN} bond lengths in CdO = 2.35 Å).

Concerning the EFG tensor, in the case of Cd localized at site D, the structural relaxation has a minor effect on the EFGs. However, for Cd at site C, the structural relaxation changes the magnitude and sign of V_{zz} and the asymmetry of the EFG tensor. As can be seen in Fig. 9, when the relaxed positions of the Cd-O_{NN} are taken into account the overall agreement of the APW + lo systematics with the experimental one is good.

To evaluate the possible contribution of the Ln-$4f$ electrons to the EFG at the Cd sites, we performed LSDA + U calculations using a value of $U = 10.9$ eV for the $4f$ electrons (the same value as in the case of the pure systems). The LSDA + U predictions for the Cd-O_{NN} bond lengths and the EFGs are the same as those obtained using LSDA (differences are on the order of the convergence error), showing that the application of the U correction to the Ln-$4f$ levels does not affect the EFG at the Cd sites.

To better understand the role of the Ln-$4f$ electrons on the EFG at the Cd sites, we performed a second study, which does not require the introduction of the U correction: we replaced the Ln constituents of the relaxed structure of $Ln_{1.875}Cd_{0.125}O_3$ with In or La (cations that do not have f electrons), fixing their atomic positions at the relaxed ones, and we calculated the EFG at the Cd sites. As an example of these calculations, in the case of Cd-doped Dy_2O_3 we obtained for Cd at site C $V_{zz}^{LSDA} = 4.7 \times 10^{21}$ V/m^2 and $\eta^{LSDA} = 0.70$, and we obtained $V_{zz}^{LSDA} = 6.5 \times 10^{21}$ V/m^2 and $\eta^{LSDA} = 0$ for Cd at site D. When Dy atoms were replaced with In, we found $V_{zz}^{LSDA} = 5.0 \times 10^{21}$ V/m^2 and $\eta^{LSDA} = 0.71$ for site C and $V_{zz}^{LSDA} = 6.8 \times 10^{21}$ V/m^2 and $\eta^{LSDA} = 0$ for site D. When the Dy atoms were replaced by La, we found $V_{zz}^{LSDA} = 4.7 \times 10^{21}$ V/m^2 and $\eta^{LSDA} = 0.71$ for site C and $V_{zz}^{LSDA} = 7.0 \times 10^{21}$ V/m^2 and $\eta^{LSDA} = 0$ for site D. From these results, it is clear that the substitution of the Dy atoms

TABLE III. LSDA + *U* predictions for V_{zz} (in units of 10^{21} V/m^2) and η at Cd impurities substitutionally located at cationic sites of Ln_2O_3 (relaxed and unrelaxed structures) compared with experimental PAC results at $T \approx 700$ K.[a]

		Site C[b]			Site D[c]		
		d(Cd-O_{NN})	V_{zz}	η	d(Cd-O_{NN})	V_{zz}	η
Gd_2O_3:Cd	Unrelaxed	2.28, 2.32, 2.41	−2.5	0.52	2.29	7.9	0.00
	Relaxed	2.32, 2.45, 2.54	4.7	0.60	2.42	6.5	0.00
	Exp.[14]		3.54(5)	0.86(1)		7.37(5)	0.00
Dy_2O_3:Cd	Unrelaxed	2.25, 2.29, 2.35	−3.4	0.62	2.30	7.5	0.00
	Relaxed	2.33, 2.45, 2.49	4.9	0.70	2.37	7.1	0.00
	Exp.[16]		4.11(2)	0.80(1)		7.52(2)	0.00
Tm_2O_3:Cd	Unrelaxed	2.23, 2.23, 2.34	−2.2	0.53	2.24	8.0	0.00
	Relaxed	2.25, 2.38, 2.39	5.4	0.71	2.27	7.3	0.00
Yb_2O_3:Cd	Unrelaxed	2.20, 2.24, 2.30	−3.3	0.47	2.25	7.2	0.00
	Relaxed	2.27, 2.37, 2.40	4.9	0.82	2.33	7.2	0.00
	Exp.[16]		4.73(5)	0.76(1)		7.57(5)	0.00
Lu_2O_3:Cd	Unrelaxed	2.18, 2.24, 2.28	−2.2	0.81	2.25	7.8	0.00
	Relaxed	2.25, 2.36, 2.40	5.1	0.75	2.33	7.4	0.00
	Exp.[18]		4.75(1)	0.743(6)		7.67(2)	0.07(3)

[a]d(Cd-O_{NN}) are the distances in angstroms from Cd to its O_{NN}.
[b]Each d(Cd-O_{NN}) value has multiplicity of two in the case of site C.
[c]Each d(Cd-O_{NN}) value has multiplicity of six in the case of site D.

by In or La atoms does not produce significant changes of the EFG at Cd sites. Similar results were obtained in other Ln sesquioxides. In conclusion, the EFG at the Cd sites is "short sighted" to the type of next-nearest neighbors and, in consequence, to the $4f$ electrons of the Ln elements.

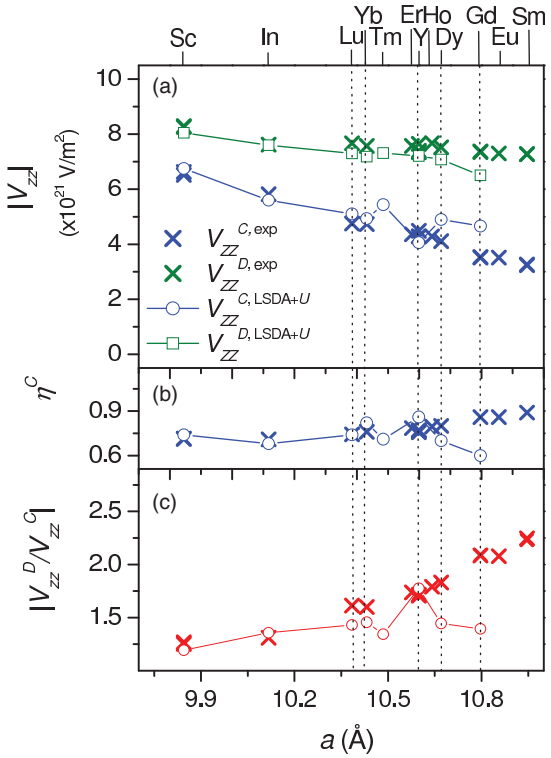

FIG. 9. (Color online) Experimental and LSDA + *U* EFG results for Cd-doped Sc_2O_3, In_2O_3, and Ln_2O_3 compounds as a function of a (respective indigenous cations are indicated on the top). (a) $|V_{zz}^C|$ and $|V_{zz}^D|$, (b) η^C, and (c) $|V_{zz}^D/V_{zz}^C|$. Crosses and open symbols correspond to experimental and LSDA + *U* results, respectively. *Ab initio* results in Y_2O_3 and In_2O_3 and in Sc_2O_3 are those reported in Refs. 19 and 64, respectively. Experimental results were extracted from Refs. 16–19 and correspond to those measurements at $T \approx$ 700 K. The dashed vertical lines were included for a visual guide.

VI. CONCLUSIONS

We have performed an *ab initio* APW + lo study of the electronic, structural, and hyperfine properties of pure and Cd-doped Ln_2O_3 using LSDA and LSDA + *U*.

In the case of the pure systems, the calculated energy band gaps are smaller than the measured ones, reflecting the well-known deficiency of LSDA. LSDA also predicts a Ln-f band at E_F, in disagreement with the experimental results. LSDA + *U* splits this f band away from E_F. The calculated DOS using LSDA + *U* shows that the conduction band is composed mainly of Ln-4f and Ln-d states while the valence band has a mainly O-p character, and the correct insulating ground state of these oxides is predicted. For both approximations, only a small hybridization between bands was found, in agreement with the picture of these sesquioxides as ionic insulators with some degree of covalent bonding between cations and oxygen.

Concerning the EFG tensor, LSDA and LSDA + *U* predict qualitatively similar systematics for the EFG at both cationic sites for the Ln series. Our LSDA calculations predict a dominating Ln-p contribution to the EFG at both cationic sites, a result that can be explained by the r^{-3} dependence of the EFG from the charge sources: even a small asymmetry of the p shell in a region close to the nucleus where the EFG is calculated (or measured) produces a strong contribution to the EFG. LSDA also predicts that V_{zz}^{pp} and V_{zz}^{ff} have opposite signs and that the magnitude of both contributions monotonously decreases with increasing a, at both C and D sites, maintaining a nearly constant V_{zz} value through the Ln series. In the case of LSDA + *U*, for some sesquioxides, the magnitudes of V_{zz}^{pp} and V_{zz}^{ff} are comparable.

For the cases of Sc_2O_3, In_2O_3, and Lu_2O_3, our predictions for the EFG tensor are in excellent agreement with the experimental results. Good agreement was also observed in the case of Gd_2O_3 and Dy_2O_3. For Tm_2O_3, the agreement with experimental EFG mesurements is poor: the predicted EFG is smaller than the experimental one at both cationic sites, but the ratio $|V_{zz}^D|/|V_{zz}^C|$ is in good agreement with the experiment. Based on this fact, the discrepancy could be attributed to an incorrect value of the nuclear quadrupole moment Q of the sensitive state of ^{169}Tm or to a bad description of the electronic structure of this system by LSDA and even by LSDA + U. A determination of this Q value could be of great interest in order to solve the controversy. The case of Yb_2O_3 is more controversial. The interaction assignment reported in the literature does not follow the experimental trend observed in other bixbyites, and APW + lo using LSDA or LSDA + U fails to predict the EFG at both cationic sites of Yb_2O_3 at low temperatures. Only for $T > 750$ K are the experimental results in agreement with the symmetry of the cationic sites of the bixbyite structure. Also, the ratio $|V_{zz}^D|/|V_{zz}^C|$ agrees with the results obtained in other Ln sesquioxides. In our opinion, progress in the understanding of this and other Ln sesquioxides (in particular Tm_2O_3) should come from experiments that could determine the magnitude, symmetry, and sign of the EFG as a function of measuring temperature. Calculations based on different methods (e.g., considering the ground state multiplets and the effect of local crystal fields on those) will be valuable for understanding of the electronic structure (and the $4f$ configuration) of Yb_2O_3.

In the case of Cd-doped bixbyites, the DOSs predicted by LSDA and LSDA + U are similar to those obtained for the pure systems, but in a behavior similar to what has been observed in other binary oxides, Cd introduces a half-occupied acceptor impurity level at E_F. In this paper, we found that the best description of hyperfine parameters is obtained by assuming the impurity level is fully occupied, in agreement with conclusions from previous studies. Concerning structural properties, the substitution of an indigenous Ln atom by a Cd impurity induces significant structural distortions in the host lattice. The enhancement of the Cd-O_{NN} bond lengths was observed in other binary oxides and suggests that Cd tends to reconstruct the bond length that it has in CdO. Our *ab initio* calculations using the APW + lo method successfully predict the experimental EFGs at Cd impurities in bixbyites and have established that the influence of the $4f$ electrons on the EFGs at Cd impurity sites is negligibly small, while the effects of structural relaxations are significant.

ACKNOWLEDGMENTS

This paper was partially supported by Consejo Nacional de Investigaciones Científicas y Técnicas (CONICET) under Project No. PIP 0002. This research made use of the HP-Parallel-Computing Bose Cluster, and the computational facilities of the Physics of Impurities in Condensed Matter group, at Instituto de Física La Plata (IFLP) and Departamento de Física (UNLP). We gratefully acknowledge Dominic H. Ryan for fruitful discussions at the first stages of this paper.

*richard@fisica.unlp.edu.ar

[1] G. Adachi and N. Imanaka, Chem. Rev. **98**, 1479 (1998).
[2] M. Tang, P. Lu, J. Valdez, and K. Sickafus, J. Appl. Phys. **99**, 063514 (2006).
[3] B. Antic, M. Mitric, and D. Rodic, J. Magn. Magn. Mater. **145**, 349 (1995).
[4] V. Srikanth, A. Sato, J. Yoshimoto, J. H. Kim, and T. Ikegami, Cryst. Res. Technol. **29**, 981 (1994).
[5] B. M. E. Russbueldt and W. F. Hoelderich, J. Catal. **271**, 290 (2010), and references therein.
[6] L. Laversenne, Y. Guyot, C. Goutaudier, M. Th. Cohen-Adad, and G. Boulon, Opt. Mater. **16**, 475 (2001); J. Zarembowitch, J. Gouteron, and M. Lejus, J. Raman Spectrosc. **9**, 263 (1980); Y. Fujimoto, T. Yanagida, Y. Yokota, A. Ikesue, and A. Yoshikawa, Opt. Mater. **34**, 448 (2011), and references therein.
[7] K. Kakushima, K. Tsutsui, S. Ohmi, P. Ahmet, V. Ramgopal Rao, and H. Iwai, Top. Appl. Phys. **106**, 345 (2007).
[8] N. N. Greenwood and T. C. Gibb, *Mössbauer Spectroscopy* (Chapman & Hall, London, 1971), Chap. 17.
[9] See, e.g., E. N. Kaufmann and R. J. Vianden, Rev. Mod. Phys. **51**, 161 (1979); H. Frauenfelder and R. M. Steffen, in *Alpha-, Beta-, and Gamma-Ray Spectroscopy*, edited by K. Siegbahn (North-Holland, Amsterdam, 1966), Vol. 2, p. 997; R. S. Raghavan, E. N. Kauffmann, and P. Raghavan, Phys. Rev. Lett. **34**, 1280 (1975); G. Schatz and A. Weidinger, *Nuclear Condensed Matter Physics—Nuclear Methods and Applications* (Wiley, Chichester, UK, 1996).
[10] T. P. Das and E. L. Hahn, *Nuclear Quadrupole Resonance Spectroscopy*, Suppl. 1 to Solid State Physics (Academic Press, New York, 1958).
[11] J. Desimoni, A. G. Bibiloni, L. A. Mendoza-Zélis, A. F. Pasquevich, F. H. Sánchez, and A. López-García, Phys. Rev. B **28**, 5739 (1983).
[12] W. Bolse, M. Uhrmacher, and K. P. Lieb, Phys. Rev. B **36**, 1818 (1987).
[13] A. Bartos, K. P. Lieb, A. F. Pasquevich, M. Urhmacher, and ISOLDE Collaboration, Phys. Lett. A **157**, 513 (1991).
[14] J. Shitu, D. Wiarda, T. Wenzel, M. Urhmacher, K. P. Lieb, S. Bedi, and A. Bartos, Phys. Rev. B **46**, 7987 (1992).
[15] D. Lupascu, A. Bartos, K. P. Lieb, and M. Urhmacher, Z. Phys. B **93**, 441 (1994).
[16] J. A. Shitu, Ph.D. thesis, Universidad Nacional de La Plata, La Plata, Argentina, 1995.
[17] J. Shitu, A. F. Pasquevich, A. G. Bibiloni, M. Rentería, and F. G. Requejo, Mod. Phys. Lett. B **12**, 281 (1998).
[18] L. A. Errico, M. Rentería, A. G. Bibiloni, and F. G. Requejo, Hyperfine Interact. **120/121**, 457 (1999).
[19] E. L. Muñoz, Ph.D. thesis, Universidad Nacional de La Plata, La Plata, Argentina, 2011.
[20] J. P. Perdew and Y. Wang, Phys. Rev. B **45**, 13244 (1992).
[21] V. I. Anisimov, J. Zaanen, and O. K. Andersen, Phys. Rev. B **44**, 943 (1991); V. I. Anisimov, I. V. Solovyev, M. A. Korotin, M. T. Czyżyk, and G. A. Sawatzky, *ibid.* **48**, 16929 (1993).
[22] W. M. Temmerman, A. Svane, Z. Szotek, and H. Winter, in *Electronic Density Functional Theory: Recent Progress and New*

Directions, edited by J. F. Dobson, G. Vignale, and M. P. Das (Plenum, New York, 1998), p. 327; W. M. Temmerman, A. Svane, Z. Szotek, H. Winter, and S. Beiden, in *Electronic Structure and Physical Properties of Solids: The Uses of the LMTO Method*, edited by H. Dreyss (Springer-Verlag, Berlin, 2000), Vol. 535, p. 286.

[23] N. V. Skorodumova, R. Ahuja, S. I. Simak, I. A. Abrikosov, B. Johansson, and B. I. Lundqvist, Phys. Rev. B **64**, 115108 (2001); S. Fabris, S. Gironcoli, S. Baroni, G. Vicario, and G. Balducci, *ibid.* **71**, 041102(R) (2005); N. Hirosaki, S. Ogata, and C. Kocer, J. Alloys Compd. **351**, 31 (2003); L. Marsella and V. Fiorentini, Phys. Rev. B **69**, 172103 (2004); L. Petit, A. Svane, Z. Szotek, and W. M. Temmerman, *ibid.* **72**, 205118 (2005); M. Mikami and S. Nakamura, J. Alloys Compd. **408-412**, 687 (2006); N. Singh, S. Mohan Saini, T. Nautiyal, and S. Auluck, J. Appl. Phys. **100**, 083525 (2006); A. Walsh, J. L. F. Da Silva, S. H. Wei, C. Korber, A. Klein, L. F. J. Piper, A. DeMasi, K. E. Smith, G. Panaccione, P. Torelli, D. J. Payne, A. Bourlange, and R. G. Egdell, Phys. Rev. Lett. **100**, 167402 (2008); F. X. Zhang, M. Lang, J. W. Wang, U. Becker, and R. C. Ewing, Phys. Rev. B **78**, 064114 (2008); P. D. C. King, T. D. Veal, F. Fuchs, Ch. Y. Wang, D. J. Payne, A. Bourlange, H. Zhang, G. R. Bell, V. Cimalla, O. Ambacher, R. G. Egdell, F. Bechstedt, and C. F. McConville, *ibid.* **79**, 205211 (2009); H. Jiang, R. I. Gomez-Abal, P. Rinke, and M. Scheffler, Phys. Rev. Lett. **102**, 126403 (2009); M. Rahm and N. V. Skorodumova, Phys. Rev. B **80**, 104105 (2009).

[24] D. Torumba, V. Vanhoof, M. Rots, and S. Cottenier, Phys. Rev. B **74**, 014409 (2006).

[25] L. Eyring, in *Handbook on the Physics and Chemistry of Rare Earths*, edited by K. A. Gschneidner Jr. and L. Eyring (North-Holland, Amsterdam, 1979), Vol. 3, p. 337.

[26] P. Villars and L. D. Calvert, *Pearson's Handbook of Crystallographic Data for Intermetallic Phases*, 2nd ed. (ASM International, Materials Park, OH, 1991).

[27] H. R. Hoekstra and K. A. Gingerich, Science **146**, 1163 (1964).

[28] M. Zinkevich, Prog. Mater. Sci. **52**, 597 (2007).

[29] R. W. G. Wyckoff, *Crystal Structures* (Wiley, New York, 1964), Vol. 2, Chap. 5.

[30] P. Hohenberg and W. Kohn, Phys. Rev. **136**, B864 (1964); W. Kohn and L. J. Sham, *ibid.* **140**, A1133 (1965).

[31] E. Sjöstedt, L. Nordström, and D. J. Singh, Solid State Commun. **114**, 15 (2000); G. K. H. Madsen, P. Blaha, K. Schwarz, E. Sjöstedt, and L. Nordström, Phys. Rev. B **64**, 195134 (2001); see also S. Cottenier, *Density Functional Theory and the Family of (L)APW-Methods: A Step-by-Step Introduction* (KU Leuven, Leuven, Belgium, 2002).

[32] P. Blaha, K. Schwarz, G. Madsen, D. Kvasnicka, and J. Luitz, *WIEN2k: An Augmented Plane Wave + Local Orbitals Program for Calculating Crystal Properties* (Vienna University of Technology, Vienna, Austria, 2012).

[33] Z. Wu and R. E. Cohen, Phys. Rev. B **73**, 235116 (2006).

[34] J. P. Perdew, A. Ruzsinszky, G. I. Csonka, O. A. Vydrov, G. E. Scuseria, L. A. Constantin, X. Zhou, and K. Burke, Phys. Rev. Lett. **100**, 136406 (2008).

[35] R. C. Albers, N. E. Christensen, and A. Svane, J. Phys.: Condens. Matter **21**, 343201 (2009).

[36] S. K. Mohanta, S. N. Mishra, S. K. Srivastava, and M. Rots, Solid State Commun. **150**, 1789 (2010).

[37] P. Blaha, K. Schwarz, and P. H. Dederichs, Phys. Rev. B **37**, 2792 (1988); K. Schwarz, C. Ambrosch-Draxl, and P. Blaha, *ibid.* **42**, 2051 (1990).

[38] L. A. Errico, M. Rentería, G. Fabricius, and G. N. Darriba, Hyperfine Interact. **158**, 63 (2004).

[39] D. Richard, E. L. Muñoz, T. Butz, L. A. Errico, and M. Rentería, Phys. Rev. B **82**, 035206 (2010).

[40] L. A. Errico, M. Rentería, A. G. Bibiloni, and G. N. Darriba, Phys. Status Solidi A **2**, 3576 (2005).

[41] J. P. Perdew, Int. J. Quantum Chem. **28**, 497 (1985); **30**, 451(E) (1986).

[42] B. M. Angelov, J. Phys. C **10**, L505 (1977); **15**, L239 (1982).

[43] A. V. Prokofiev, A. I. Shelykh, and B. T. Melekh, J. Alloys Compd. **242**, 41 (1996).

[44] F. Hanic, M. Hartmanová, G. G. Knab, A. A. Urusovskaya, and K. S. Bagdasarov, Acta Crystallogr. B **40**, 76 (1984), and references therein.

[45] S. Stecura and W. J. Campbell, *Thermal Expansion and Phase Inversion of Rare-Earth Oxides*, Bureau of Mines Report No. 5847 (United States Department of the Interior, Washington, 1961).

[46] N. Maslen, V. A. Streltsov, and N. Ishizawa, Acta Crystallogr. B **52**, 414 (1996).

[47] A. Saiki, N. Ishizawa, N. Mizutani, and M. Kato, J. Ceram. Soc. Jpn. **93**, 649 (1985).

[48] M. D. Alba, P. Chain, P. Florian, and D. Massiot, J. Phys. Chem. C **114**, 12125 (2010).

[49] G. K. Semin, Russ. J. Phys. Chem. A **81**, 38 (2007), and references therein.

[50] J. D. Cashion, D. B. Prowse, and A. Vas, J. Phys. C: Solid State Phys. **6**, 2611 (1973).

[51] D. W. Forester and W. A. Ferrando, Phys. Rev. B **14**, 4769 (1976).

[52] G. A. Stewart, R. K. Day, J. B. Dunlop, and D. C. Price, Hyperfine Interact. **40**, 339 (1988).

[53] K. G. Plingen, B. Wolbeck, and F. J. Schröder, Nucl. Phys. A **165**, 97 (1971).

[54] C. Meyer, J. P. Sanchez, J. Thomasson, and J. P. Itié, Phys. Rev. B **51**, 12187 (1995).

[55] M. Rams, Diploma Thesis, Jagiellonian University, Kraków, Poland, 1996; M. Rams and K. Królas, in *Proceedings of the XXXII Zakopane School of Physics* (Kraków, Poland, 1997), p. 401.

[56] N. J. Stone, At. Data Nucl. Data Tables **90**, 75 (2005).

[57] A. F. Pasquevich, A. G. Bibiloni, C. P. Masssolo, M. Rentería, J. A. Vercesi, and K. Freitag, Phys. Rev. B **49**, 14331 (1994).

[58] R. L. Mössbauer, Rev. Mod. Phys. **36**, 362 (1964).

[59] M. Forker, Hyperfine Interact. **24-26**, 907 (1985).

[60] H. H. Wickman and I. Nowik, J. Phys. Chem. Solids **28**, 2099 (1967).

[61] E. Gerdau, H. Winkler, and F. Sabathil, in *AIP Conference Proceedings* (AIP, Argonne, IL, 1977), Vol. 38, p. 35; Hyperfine Interact. **4**, 630 (1978).

[62] J. M. Cadogan and D. H. Ryan, Hyperfine Interact. **153**, 25 (2004).

[63] T. J. Bastow, Solid State Nucl. Magn. Reson. **3**, 17 (1994).

[64] E. L. Muñoz, D. Richard, L. A. Errico, and M. Rentería, Physica B **404**, 2757 (2009).

[65] L. A. Errico, G. Fabricius, M. Rentería, P. de la Presa, and M. Forker, Phys. Rev. Lett. **89**, 055503 (2002).

[66] L. A. Errico, G. Fabricius, and M. Rentería, Phys. Rev. B **67**, 144104 (2003).

[67] G. N. Darriba, M. Rentería, H. M. Petrilli, and L. V. C. Assali, Phys. Rev. B **86**, 075203 (2012).